Non-Gaussian Photon Probability Distribution

Benjamin T. Solomon

iSETI LLC
P.O. Box 831
Evergreen, CO 80437
303-618-2800; benjamin.t.solomon@iseti.us

Abstract. This paper investigates the axiom that the photon's probability distribution is a Gaussian distribution. The Airy disc empirical evidence shows that the best fit, if not exact, distribution is a modified Gamma $m\Gamma$ distribution (whose parameters are $\alpha = r$, $\beta = r/\sqrt{u}$) in the plane orthogonal to the motion of the photon. This modified Gamma distribution is then used to reconstruct the probability distributions along the hypotenuse from the pinhole, arc from the pinhole, and a line parallel to photon motion. This reconstruction shows that the photon's probability distribution is not a Gaussian function. However, under certain conditions, the distribution can appear to be Normal, thereby accounting for the success of quantum mechanics. This modified Gamma distribution changes with the shape of objects around it and thus explains how the observer alters the observation. This property therefore places additional constraints to quantum entanglement experiments. This paper shows that photon interaction is a multi-phenomena effect consisting of the probability to interact P_i, the probabilistic function and the ability to interact A_i, the electromagnetic function. Splitting the probability function P_i from the electromagnetic function A_i enables the investigation of the photon behavior from a purely probabilistic P_i perspective. The Probabilistic Interaction Hypothesis is proposed as a consistent method for handling the two different phenomena, the probability function P_i and the ability to interact A_i, thus redefining radiation shielding, stealth or cloaking, and invisibility as different effects of a single phenomenon P_i of the photon probability distribution. Sub wavelength photon behavior is successfully modeled as a multi-phenomena behavior. The Probabilistic Interaction Hypothesis provides a good fit to Otoshi's (1972) microwave shielding, Schurig *et al.* (2006) microwave cloaking, and Oulton *et al.* (2008) sub wavelength confinement; thereby providing a strong case that the photon probability distribution is a modified Gamma $m\Gamma$ distribution and not a Gaussian distribution.

Keywords: Photon Probability, Sub Wavelength, Quantum Entanglement, Shielding, Cloaking, Invisibility, Stealth
PACS: 14.70.Bh, 32.80.Rm, 33.20.Bx, 42.50.Ct, 78.70.-g)

INTRODUCTION

Solomon (2009) had proposed that elementary particles obey Internal Structure Independence, that acceleration was independent of the internal properties or structure, whether quantum-mechanical, string or some other theoretical approach. Realism (Eisaman *et al.,* 2008) requires that physical observations are properties possessed by the system whether observed or not. One can add that realism is dependent upon our *interpretations of observations* and *inferences of the unobserved*. Revisiting the established Airy disc experimental observations this paper proposes a different *interpretation of observations* that the photon probability distribution is a modified Gamma distribution $m\Gamma$ and not a Gaussian distribution.

To support this modified Gamma $m\Gamma$ distribution finding this paper proposes the Probabilistic Interaction Hypothesis as a framework of consistent relationships that are determined by the shape of the space around a photon. That is, there are two independent phenomena the ability to interact with a material and the probability of interacting with a material and a variable, the environment, the shape of space around the photon. It is then shown that shielding, cloaking, invisibility are single phenomenon effects of the photon probability distribution. To test for multi-phenomena behavior this paper explores sub-wavelength properties as a function of both the modified Gamma probability distribution and the electric field. This modified Gamma $m\Gamma$ approach is in good agreement with the experimental results, thus providing a strong case for both the modified Gamma $m\Gamma$ distribution and the framework for using this distribution in a multi-phenomena environment.

INFERRED CHARACTERISTICS OF THE PHOTON PROBABILITY DISTRIBUTION

In the Airy pattern experiment, Figure 1(a), the intensity of the photons passing through a pinhole, and hitting the visual plane screen is given by the equations (1), (2) and (3) where I is the transmitted intensity of light on the visual plane as a function of the angle θ, the angle between the perpendicular from pinhole and screen, to the hypotenuse from the pinhole, I_O is reference intensity, λ is wavelength of light photon, D_A is aperture diameter of the pinhole, D_P is distance between pinhole and screen, and r is radius of the Airy pattern concentric circle on the screen.

$$I = I_O \sin(u)/u \tag{1}$$

$$u = \pi/\lambda . D_A \sin(\theta) \tag{2}$$

$$\tan(\theta) = r/D_P \tag{3}$$

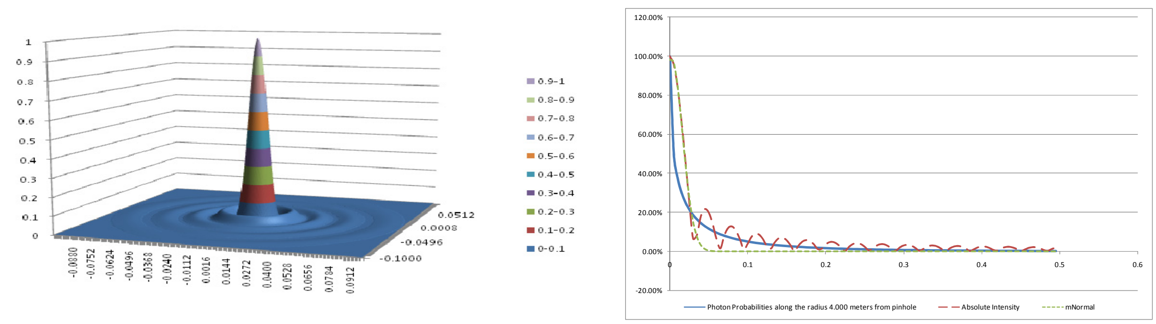

(a) **(b)**

Figure 1. (a) Photon intensity of an Airy disk and its concentric rings and (b) comparisons of intensity with Gamma & Normal distributions.

The intensity I can be interpreted as a function of the probability of the photon energy as for a specific photon frequency the intensity is a direct function of the number of photons and therefore a direct indicator of the photon's probability distribution. The Airy pattern with its concentric rings suggests a radial probability density function. This distribution can be extracted by normalizing the area under equation (1) to unity. Equation (2) can be rewritten as,

$$u = \pi/\lambda . D_A (r/s) = \pi/\lambda . D_A \left(r/\sqrt{r^2 + {D_P}^2} \right) \tag{4}$$

where s is the slope or hypotenuse of the triangle formed by the distance D_P from the pinhole and radius r on that orthogonal visual plane. By equation (1) the intensity I is constant for a specific angle θ. By equation (4), intensity I forms isolines or 'isocircles' of equal intensities. Therefore, the photon probability distribution is axisymmetric. This axisymmetry implies radial amplitude modulation of intensity is a function of wavelength, equation (2), due to the wave nature interfering constructively and destructively on the probability distribution. One infers that there is a two-step process at work here. First, the energy intensity is determined by the probability density function. Second, the wave nature then distorts the probability distribution and therefore, the energy intensity to form concentric rings.

In essence the wave function casts a 'shadow' (for the want of a better term) on the probability function. This behavior is inferred from the fact that the wavelength is of the order of 10^{-7}m but the intensity function and therefore the probability distribution is of the order of 10^{-2}m to 10^{1}m; a difference of 5 to 8 orders of magnitude. This shadow effect suggests two properties. First, that the source of the photon's probability distribution is somehow enclosed by the electromagnetic field structure and second, that the probability distribution and electromagnetic field are able to interact with each other. Using this two-step process one can subtract out the wave function from the Airy pattern to leave a pure probability function. Therefore one cannot use equation (1) to determine the photon probability function as it is a function of both, the probability distribution and the wave nature. Figure 1(b) illustrates the approach used to remove the effect of the wave nature on the probability distribution. A smooth continuous function was fitted over *absolute values* of the normalized intensity data. Two approaches were used to arrive at the final solution. First, to narrow the type of distribution most likely to fit the data, Palisade's @RISK was used to fit known distributions to 11 intensity data sets from different experimental parameters. Second, further curve fitting of the data was conducted to minimize the error sum of squares. The distribution that best fitted the intensity data set on the visual plane is the Gamma distribution, equation (5), where $\alpha > 0$ and $\beta > 0$ are the continuous shape & scale parameters respectively. The mean and variance of are given by $\alpha\beta$ and $\alpha\beta^2$respectively. Figure 1(b) presents one result of this analysis for $\lambda=5.5x10^{-7}m$, $D_A=5x10\text{-}5m$, $D_P = 4m$. It shows that the photon's orthogonal probability distribution is a too fat and long tailed to be Normal. Figure 1(b) shows that the standard deviation of the Normal is about 0.02 while the Gamma's tail reaches 0.5 or 25 Normal standard deviations.

$$f(r) = \frac{1}{\beta\Gamma(\alpha)}\left(\frac{r}{\beta}\right)^{\alpha-1} e^{-r/\beta} \tag{5}$$

Quantum mechanics is based on the Gaussian distribution, and this distribution was fitted to the same 10,000 data points, Figure 1(b). The best fit Gaussian distribution, equation (6), is with $a=0.9907$, $b= 0.4976$, $c= -0.0984$. Solving for the Normal mean and standard deviation does not give a unique solution. However, sensitivity analysis suggests that $a=1/\sigma\sqrt{(2\pi)}=1$, and $c=\mu/\sigma\sqrt{2}=0$. This implies that $\mu=0$, and that $\sigma=1/\sqrt{(2\pi)}$ but $b=1/\ \sigma\sqrt{2}\approx 0.5$. Therefore, the Normal distribution cannot be a candidate because σ cannot be both $1/\sqrt{(2\pi)}$ and $\sqrt{2}$. The photon's orthogonal distribution not a Gaussian distribution even if described as a function of the shape of the external space u around it.

$$f(u) = a.e^{-(ub-c)^2} \tag{6}$$

To precisely determine the relationship between α, β, D_A, D_P and r a 10,000 data point cross-section of the intensity function I formed by a rectangular plane sectioned by D_P and r was constructed. This intensity plane was recalculated for 19 wavelengths λ between $1x10^{-6}m$ to $1x10^{-7}m$, and for 7 different values of D_A, between $0.0001m$ to $0.0007m$ totaling 133,000 data points. The best fit relationship for α and β are given by equations (7) and (8). This Gamma distribution is determined entirely by the physical experimental set-up D_A, D_P, r and λ and is not a function of time. This distribution is better described as a modified Gamma $m\Gamma$ as its parameters are not constant terms.

$$\alpha = r \tag{7}$$

$$\beta = r/\sqrt{u} \tag{8}$$

To examine the the photon probability distribution's shape, three cross-sections of were constructed from multiple consecutive $m\Gamma$ distributions. First, a distribution along a line parallel to D_P. The best fit function was not Gaussian but of the form given by equation (9). However, this function does not always give a good fit.

$$f(D_P) = -0.861u^{0.129} + 1.324 \tag{9}$$

Second, along a hypotenuse from the pinhole to any point on the visual plane. Figure 2(a) depicts several distributions at selected angles θ from the line D_P and shows that the hypotenuse distribution appears Normal for large θ but becomes fat-tailed as θ decreases (distribution shifts right). To test for Normality, the best fit standard deviations were calculated with the means set at the peaks. The Normal provides a good fit when θ is large but not when θ is small. Figure 2(b) shows that at $\theta=84.6°$ (small dash curve) the height of the Normal mode ≈5% and agrees with the photon $m\Gamma$ distribution. When $\theta=0.9°$ (dot-dash curve) the height of the Normal's mode $<5\%$ but that of the photon $m\Gamma$ distribution is $>25\%$ and the photon's spread is several times that of the Normal's. Third, the probability distribution along an arc at selected distances from the pinhole, Figure 2(c). None of these distributions are Gaussian. Thus there are three reasons for quantum mechanics success. First, by the law of large numbers, the average behavior of a photon is always Normal. Second, for large α, the gamma distribution converges to Gaussian distribution with mean $\mu = \alpha\beta$ and variance $\sigma^2 = \alpha\beta^2$. That is when $r \gg \lambda$ the Normal distribution $N(\alpha\beta,\sqrt{\alpha\beta^2})$ is a good representation of the photon's orthogonal distribution. And third, above a certain threshold angle of about 40° the photon's hypotenuse probability distribution can be modeled by a Normal distribution.

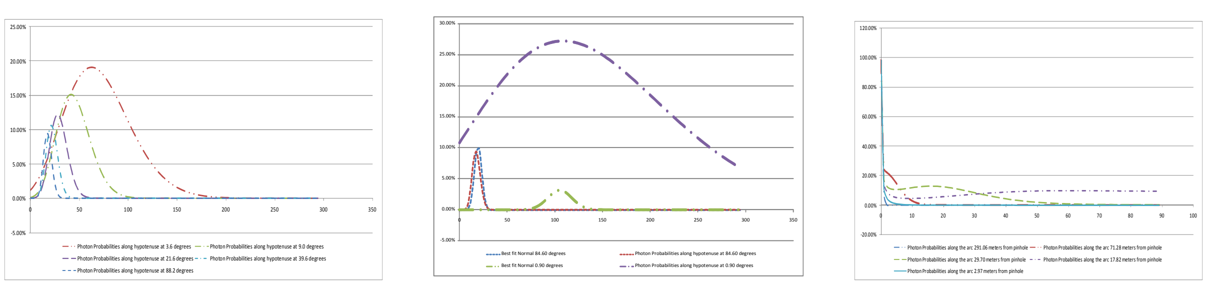

(a) (b) (c)

Figure 2. (a) Probability distribution along the hypotenuse, (b) comparisons hypotenuse distributions and (c) photon probability distribution along an arc.

THE SHAPE OF THE PHOTON'S PROBABILITY DISTRIBUTION

Figure 2(a) illustrates another characteristic, the mode of the distribution moves outward (to the right) as the angle θ is reduced. In this example, when $\theta \approx 0$ (red double dot-dash curve) the mode is 62.4 m from the pinhole, begging the question what is the true shape of the photon's probability distribution? *1%* probability was used to set the dimensional parameters. The maximum radius $R_{1\%}$ at any point from D_P is determined when the photon distribution reduces to *1%*. Similarly, the distribution's length $L_{1\%}$ is the length along D_P when the probability reduces to *1%*. Figure 3(a) illustrates a typical shape of the photon's *1%* distribution along D_P which approximates a fat-tailed lognormal. Figure 3(b) illustrates the maximum probability at any D_P for a given radius r. In this example the photon's length $L_{1\%}=4{,}900m$ long. The photon's mode is 39m from the pinhole, and the maximum radius $R_{1\%}=34.1m$ from the axis of motion. This is a huge size compared to the wavelength of $1x10^{-6}m$ to $1x10^{-7}m$. In view of this size quantum entanglement experiments need to be redesigned as it just may be that entangled photons exhibit non-locality because their probability distributions physically overlap in space. Equations (7) and (8) show that this $m\Gamma$ distribution has shape changing properties, as both α and β are functions of of the space around the photon. That is D_A the radius of the orthogonal space and D_P the free space in front of the photon at the moment the photon leaves a material. Calculations show that if the space in front D_P approaches infinity this distribution can be several 100,000 km long. Figure 4(a) illustrates how the distribution narrows with aperture D_A reduction. As the aperture D_A is reduced by *25x* from *1000nm* to *40nm* the probability distribution is narrowed by *≈2x* from *4.5m* to *2.5m*. This effect is non-linear in free space. Figure 4(b) shows how the distribution shortened as D_A is reduced. D_A can be used to reduce the volume of space the photon distribution occupies. These shape changing properties would explain how an observer alters the observation by changing the shape of the space around the photon.

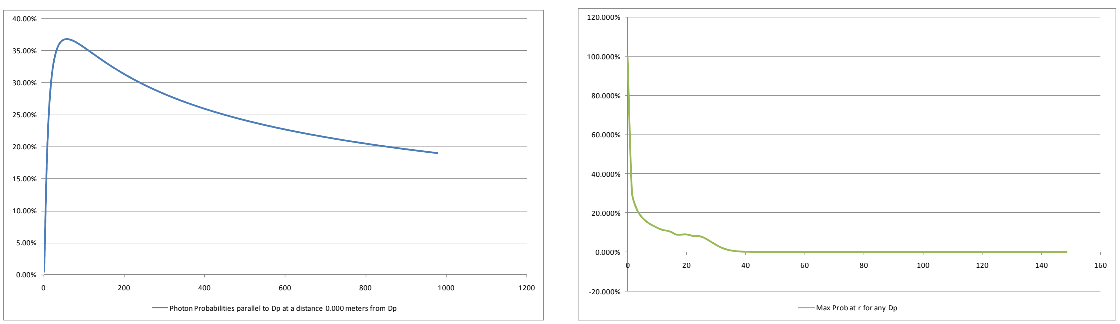

(a) **(b)**

Figure 3. (a) Typical probability shape along D_P and (b) max probability at any D_P for a given, r.

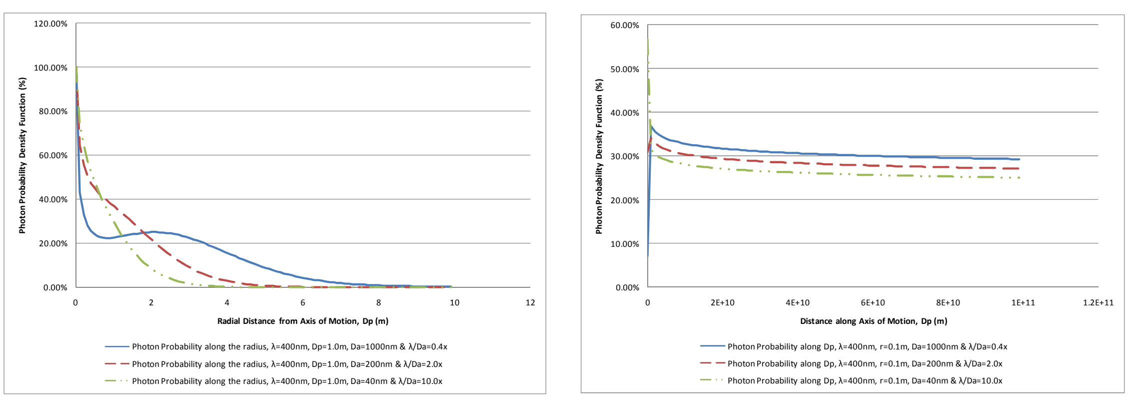

(a) **(b)**

Figure. 4. (a) The radius is reduced as D_A is reduced and (b) the length is reduced as D_A is reduced.

ADDITIONAL RESTRICTIONS FOR QUANTUM ENTANGLEMENT

Locality demands the conservation of causality, meaning that information cannot be exchanged between two space-like separated parties or actions (Eisaman *et al.,* 2008). Quantum entanglement can be described (Howell *et al.,* 2004) as non-local interactions or the idea that distant particles do interact without the hidden variables. The large size of the probability field provides an explanation for quantum entanglement without hidden variables. Entanglement occurs while the probability fields overlap, should not if they don't and can be experimentally verified. Numerically the joint probability $P_{i,j}$ equation (10) of photon i interacting with its entangled photon j is the product of the individual probabilities $P_{i,x,y,z}$ and $P_{j,x,y,z}$, at any point in space, whose coordinates are given by x,y,z. Given that these probabilities obey the modified Gamma $m\Gamma$ distribution equation (10) can be written as equation (11)

$$P_{i,j} = \sum_{x}\sum_{y}\sum_{z} P_{i,x,y,z} P_{j,x,y,z} \; ; \tag{10}$$

$$P_{i,j} = \sum_{x}\sum_{y}\sum_{z} m\Gamma_{i}(x,y,z).m\Gamma_{j}(x,y,z) \,. \tag{11}$$

A numerical model was constructed for red light $\lambda=700nm$, $\lambda/D_A=2$, $D_P=100mm$. Figure 5(a) and 5(b) show joint probability densities of two photons separated by the distances $s=20mm$ and $s=270mm$ respectively. The respective probability density fields form curved surfaces ($3.6m$ x $3.6m$ and $4.2m$ x $4.2m$) with two spikes of heights *30.6%* and *33.3%* along the photons' axis of motion. The average height of the curved surfaces drops from *≈15%* to *≈10%* as the photons are separated from $s=20mm$ to $s=270mm$ respectively. The joint probabilities reduce to zero if $s\geq 12m$. If quantum entanglement is due to the joint $m\Gamma$ probability distribution then quantum entanglement should not be observed if the horizontal separation between the two photons $>12m$ ($D_P=0.1m$).

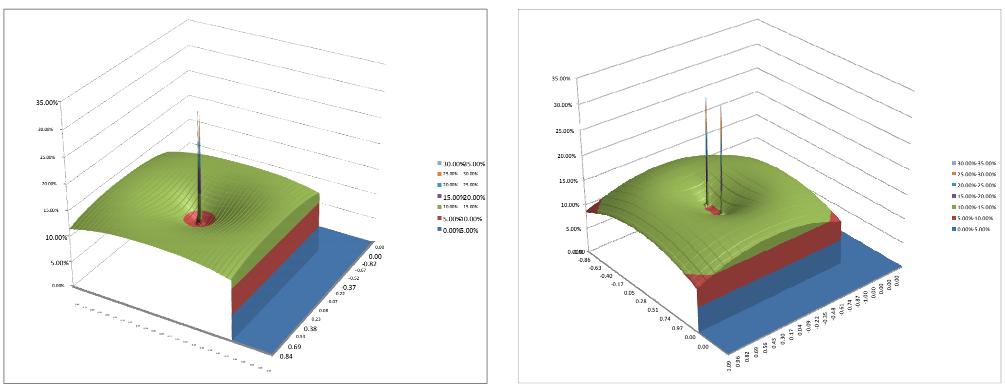

(a) **(b)**

Figure 5. (a) Entangled pdf, λ=700nm, s=20mm, $\lambda/D_A=2$ and (b) entangled pdf, λ=700nm, s=270mm, $\lambda/D_A=2$.

The work of other experimenters, (Aspect *et al.*, 1982; Howell *et al.*, 2004; Yao *et al.*, 2006; Yarnall *et al.*, 2007; Leach *et al.*, 2009) were reviewed for physical layout. Except for Howell very little information of the physical layout of these experiments are provided. Howell's experimental set up was $\leq 0.5m$ across and one infers that Aspect's and Yao's experiments were on the order of *6m* and *1m*, respectively. The exception to these experiments is Tittel *et al.* (1998) *10km* experiment in Geneva, which appears to confirm quantum entanglement at *10km* except that in this experiment returning photons and therefore overlapping probability fields were present. The $m\Gamma$ distribution provides some restrictions on physical layout of entanglement experiments. First, entangled photons travelling in parallel must be $>32m$ apart. Second, entanglement testing cannot be done when photons are coming together head on as their probability distributions overlap. Third, photons are only allowed to be reflected away from each other as reflection of the probability field is not fully understood at this time. Fourth, there can be no other reflections. And, fifth no returning photons as their probability fields would interfere with the test.

SEPARATING THE PROBABILITY FROM THE ELECTROMAGNETIC FUNCTION

Figure 6(a), illustrates a Glass Thought Experiment used to elicit several properties. Photons having passed through the transparent visual plane form Airy discs on the opaque visual plane with their respective modified Gamma distributions of $m\Gamma_t$ and $m\Gamma_o$. In the transparent visual plane, the Airy patterns are not discernable as the electromagnetic function does not interact with the visual plane. In the opaque visual plane, the electromagnetic function does interact with the visual plane to form Airy patterns. This Glass Thought Experiment illustrates several properties. First, $m\Gamma_o \neq f(m\Gamma_t)$ or the Airy patterns on the opaque visual plane demonstrate that the photon's probability distribution is intact after having passed through the transparent visual plane. Second, $m\Gamma_o \neq 0$ for any D_P or moving the opaque visual plane back and forth demonstrates that the photon probability function exists in the space between the pinhole and the opaque visual plane. Third, $A_i \neq f(P_i)$ or the electromagnetic function's ability to interact A_i with the material is independent of the photon's probability distribution or its probability to interact P_i. This is because the photon interacts ($A_i > 0$) with the opaque but not ($A_i = 0$) with the transparent visual plane even if the two planes are attached together, $m\Gamma_o = m\Gamma_t$ or when they are far apart, $m\Gamma_o \neq m\Gamma_t$. Fourth, $P_i = f(m\Gamma)$ and $P_i \neq f(A_i)$, in both visual planes the probability to interact P_i is determined by the modified Gamma distribution and not by the material. This is because the probability to interact P_i is independent of the opaque material and is even present when no interaction is observed. Ignoring edge diffraction effects to keep it simple, Figure 6(b) shows that an opaque barrier can effectively neutralize the photon probability distribution in that region where the barrier exists. Or fifth, $\int m\Gamma dr=1$, in a confined space the $m\Gamma$ distribution along a radius r has to be scaled up so that the total radial $m\Gamma$ probability is 1. Therefore, one can infer new methods of modeling photon interaction based on the $m\Gamma$ probability distribution, and test its validity. This paper proposes the Probabilistic Interaction Hypothesis that the net effect of the photon interaction I_i with a material can be modeled as equation (12) where B_i is some constant term that represents barriers to the interaction, and A_i can be described as an accelerant because it has a multiplicative effect on the probability of interaction

$$I_i = A_i f\left(P_i\right) + B_i \qquad (12)$$

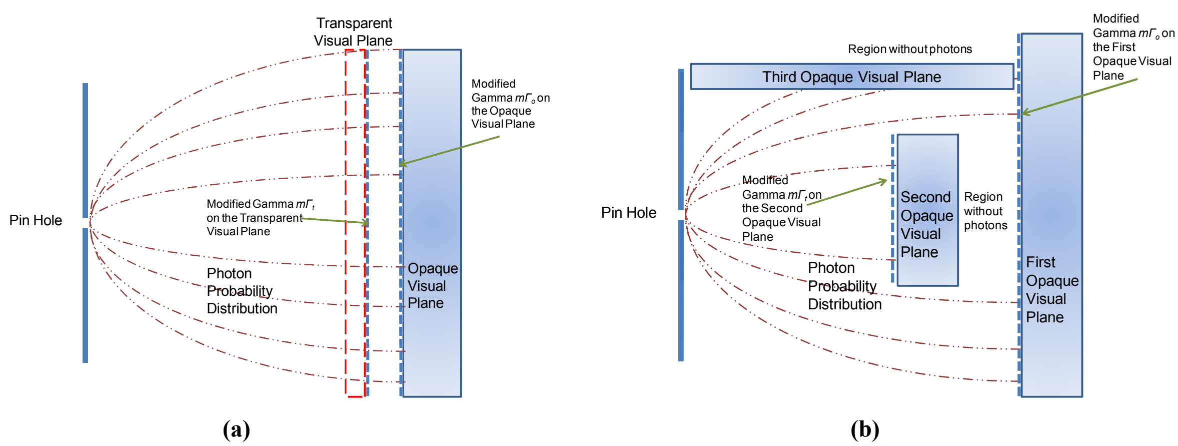

Figure 6. (a) Opaque & transparent visual plane Airy discs and (b) blocked photon probabilities.

THE SHIELDING, CLOAKING & INVISIBILITY PROBABILISTIC HYPOTHESIS

The $m\Gamma$ distribution lends itself to a unified shielding, cloaking and invisibility probabilistic hypothesis, Figure 7. These three phenomena can be defined in terms of the how the photon's probability distribution exists in the presence of objects. The cum orthogonal photon probabilities $P_{\leq r}$ is the area not under the tail or area under the $m\Gamma$ distribution from $r = 0$ to some point $r \geq 0$. The cum orthogonal photon probabilities $P_{>r}$ is the area under the tail, or area from $r > 0$ to some point $r = \infty$.

Shielding, Figure 7(a), is the ability to prevent photons slip through holes in a barrier or the probability that a photon will actualize itself within the aperture and not hit the disc. Using the Probabilistic Interaction Hypothesis, the Probabilistic Shielding Effectiveness SE_P can be defined as the ratio $P_{\leq R} / P_{\leq r}$, or the total probability over a disc of radius R to that of an aperture of radius r within the disc. Writing as decibels gives equation (13). In free space $R = \infty$, $P_{\leq R} = 1$, gives equation (14).

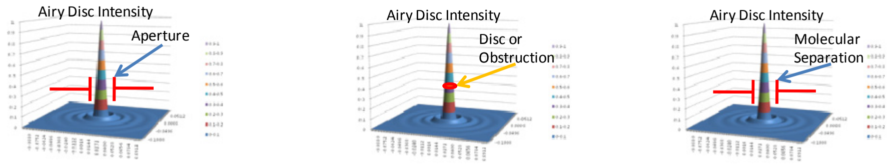

Shielding Effectiveness, SE_P, is defined as the ability to stop photon propagation through holes of radius *r* in the material. Or ratio of probability outside the hole to the total.

$$SE_P = 10\log_{10}\left[\frac{P_\infty}{P_{\le r}}\right] = 10\log_{10}\left[\frac{1}{P_{\le r}}\right]$$

(a)

Cloaking Effectiveness, CE_P, is defined as the ratio of the distribution that is present outside the obstruction of radius *r* to the total, i.e. the probability distribution that 'escapes' around the disc or obstruction.

$$CE_P = 10\log_{10}\left[\frac{P_\infty}{P_{\ge r}}\right] = 10\log_{10}\left[\frac{1}{P_{\ge r}}\right]$$

(b)

Invisibility Effectiveness, IE_P, is defined as the ability to pass through the spaces between atoms and molecules of radius *r* without interacting with the material. The ratio of the distribution that pass through the molecular separation to the total.

$$IE_P = 10\log_{10}\left[\frac{P_{\le r}}{P_\infty}\right] = 10\log_{10}\left[P_{\le r}\right]$$

(c)

Figure 7. (a) Shielding Effectiveness, (b) Cloaking Effectiveness and (c) Invisibility Effectiveness.

$$SE_P = 10\log_{10}\left[\frac{P_{\le R}}{P_{\le r}}\right]; \tag{13}$$

$$SE_P = 10\log_{10}\left[\frac{1}{P_{\le r}}\right]. \tag{14}$$

Cloaking, Figure 7(b), is the ability of photons to get around an object in its path or the probability that the photon will actualize outside the disc and not interact with the disc. Using the Probabilistic Interaction Hypothesis, the Probabilistic Cloaking Effectiveness CE_P can be defined as the ratio $P_{\le R}$ / $P_{\ge r}$, or the total probability within an aperture of radius R to that of a disc of radius r within the aperture. Writing as decibels gives equation (15). In free space $R = \infty$, $P_{\le R} = 1$, gives equation (16)

$$CE_P = 10\log_{10}\left[\frac{P_{\le R}}{P_{>r}}\right]; \tag{15}$$

$$CE_P = 10\log_{10}\left[\frac{1}{P_{>r}}\right]. \tag{16}$$

Invisibility, Figure 7(c), is the ability of photons to pass through an object without interacting with it or the probability that the photon will not actualize in a material. Using the Probabilistic Interaction Hypothesis, the Probabilistic Invisibility Effectiveness IE_P can be defined as the ratio $P_{\le r}$ / $P_{\le R}$, or the total probability over a disc of radius R to that of an aperture of radius r within the disc. Writing as decibels gives equation (17). In free space $R = \infty$, $P_{\le R} = 1$, gives equation (18)

$$IE_P = 10\log_{10}\left[\frac{P_{\le r}}{P_{\le R}}\right]; \tag{17}$$

$$IE_P = 10\log_{10}\left[P_{\le r}\right]. \tag{18}$$

Figures 8(a) and (b) illustrate the general scope of the results of these calculations in the two different scenarios, free space, and confined space, for *8,500 MHz* microwave, $R=0.10m$, and $0.0008m<r<0.1000m$. The results of the Otoshi (1972) shielding function for an equivalent porosity compares well with the Probabilistic Shielding. Writing the modified Gamma function as $m\Gamma(r)$ a function of the orthogonal radius r, $P_{\le r}$, $P_{\le R}$ and $P_{>r}$ can for the numerical integration in free space, be expressed as equations (19), (20) and (21) respectively. Where x_i is the *ith* distance between 0 and r, δr is increment in the radial distance such that x_{i+1}- $x_i = \delta r$. $2\pi x_i$ is the perimeter length at radius x_i; multiplying by δr gives the small area in which the probability is $m\Gamma(x_i)$. Note equation (21) is used to normalize the cum probability density function so that over the disc or visual plane formed by the x_i, at a distance D_P, the sum of all the probabilities adds to 1.

$$P_{\le r} = \sum_{x_i=0}^{x_i=r}\left(2\pi x_i.\delta r\right)m\Gamma(x_i); \tag{19}$$

$$P_{\le R} = \sum_{x_i=0}^{x_i=R}\left(2\pi x_i.\delta r\right)m\Gamma(x_i); \tag{20}$$

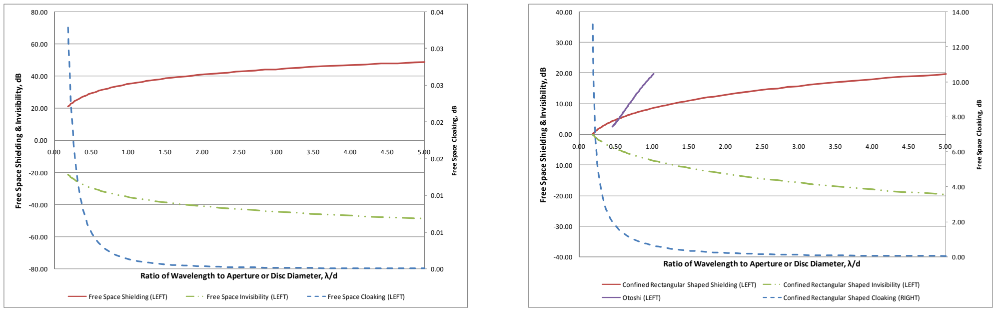

(a) **(b)**

Figure 8. (a): Free Space Probabilistic Behavior and (b) waveguide Confined Probabilistic Behavior.

$$P_{\infty} = \sum_{x_i=0}^{x_i=\infty} (2\pi x_i.\delta r)\, m\Gamma(x_i)\,; \tag{21}$$

$$P_{>r} = P_{\infty} - P_{\leq r}\,. \tag{22}$$

For the confined rectangular format of the waveguide of height h, $P_{\leq r}$, $P_{\leq R}$ and $P_{>r}$ can be expressed for the numerical integration as equations (23), (24) and (25) respectively. Where x_i is the *ith* distance between *0* and r, δr is increment in the radial distance such that $x_{i+1}- x_i = \delta r$. Equation (25) is used to normalize the cum probability density function so that the sum of all the probabilities adds to *1* where $2x_i tan^{-1}(h/x_i)$ is the arc length of radius x_i bound by the microwave cavity height h; multiplying by δr gives the small area in which the probability is $m\Gamma(x_i)$. For angle incidence θ_i, plate thickness t, for hole diameter $1.6mm < d < 12.7mm$ with horizontal and vertical spacing of a & b for a microwave with free space wavelength of λ_0. $32t/d$ is a plate thickness correction factor which is,

$$P_{\leq r} = \sum_{x_i=0}^{x_i=r} \left(2\delta r x_i.\tan^{-1}\frac{h}{x_i} \right) m\Gamma(x_i)\,; \tag{23}$$

$$P_{\leq R} = \sum_{x_i=0}^{x_i=R} \left(2\delta r x_i.\tan^{-1}\frac{h}{x_i} \right) m\Gamma(x_i)\,; \tag{24}$$

$$P_{\infty} = \sum_{x_i=0}^{x_i=\infty} \left(2\delta r x_i.\tan^{-1}\frac{h}{x_i} \right) m\Gamma(x_i)\,. \tag{25}$$

TESTING THE SHIELDING HYPOTHESIS

In microwave shielding, the microwave ability to interact with the antenna should be large A_i » *0* otherwise antennas won't function well. Otoshi (1972) presents an approximate expression for transmission loss T_{dB} for a flat perforated conductive sheet, equation (26) using a WR 430 waveguide (*431.8x109.22x54.61mm*) to investigate microwave dish antenna loss due to holes. That is larger the hole size, larger the transmission and therefore, the dish antenna loss

$$T_{dB} = 10\log_{10}\left[1 + \frac{1}{4}\left(\frac{3ab\lambda_0}{\pi d^3 \cos\theta_i} \right)^2 \right] + \frac{32t}{d}\,. \tag{26}$$

For angle of incidence θ_i, plate thickness t, for hole diameter $1.6mm < d < 12.7mm$ with horizontal and vertical spacing of a & b and microwave free space wavelength of λ_0. $32t/d$ is a plate thickness correction factor which is equivalent to the barrier term B_i in equation (12). Simplifying, for a thin wire mesh, $a=b=d$, and $t=0$, gives equation (27). The electronics industry uses an equivalent formula for slot shielding effectiveness, given by equation (28)

$$T_{dB} = 10\log_{10}\left[1 + 0.2280\left(\frac{\lambda_0}{d} \right)^2 \right]; \tag{27}$$

$$SE_L = 20\log_{10}\left[\frac{\lambda_0}{2L} \right] = 10\log_{10}\left[\left(\frac{\lambda_0}{2L} \right)^2 \right] \tag{28}$$

Table 1 and Figure 9(a) presents Otoshi's measured results with the Probabilistic Shielding, equation (13). Figure 9(b) depicts some of Otoshi's perforated sheets. The results concur with the Probabilistic Interaction Hypothesis, equation (12), with A_i of 3.95, 4.01, and 1.24 and B_i of -18.95, -16.52 and +14.67 for microwave frequencies of 2,300 MHz (rows 1-6), 2,388 MHz (rows 7-27) and 8,448 MHz (rows 28-31) respectively. The correlations are 98.39% and 95.26% for 2,300 and 2,388 MHz. It is 88.75% for 8,448 MHz. Row 31 caused the drop in correlation for 8,448 MHz. Rows 32 & 33 behave differently from the rest of the 8,448 MHz data but there is insufficient data to investigate this. To simplify the simulation all holes are rectangular. Otoshi's holes were circular, Figure 9(b). This data shows that $A_i = 24.47\lambda + 0.85$ and $B_i = -273.78\lambda + 17.28$ are functions of wavelength, and to relate this to cavity dimensions requires multiple sets of experimental data (not available at this time) with multiple waveguide cavity dimensions.

Table 1. Comparison of Otoshi (1972) experimental and theoretical results with the probabilistic hypothesis.

	Microwave Frequency (MHz)	Wavelength Λ (m)	Hole Diameter, d (m)	Ratio d/λ	32t/d	Estimated Displacement Row, a (m)	Estimated Displacement Column, b (m)	Shielding Effectiveness Actual[1] Measured (dB)	Shielding Effectiveness Probability[2] Model (dB)	Shielding Effectiveness Otoshi[3] Model (dB)	Errors Actual-Probabilistic	Errors Actual-Otoshi
1	2,300	0.1303	0.0052	0.040	0.345	0.0138	0.0167	48.00	16.67	63.44	31.33	-15.44
2	2,300	0.1303	0.0052	0.040	0.345	0.0100	0.0100	40.80	15.59	52.63	25.21	-11.83
3	2,300	0.1303	0.0091	0.070	0.197	0.0275	0.0250	40.80	14.74	55.73	26.06	-14.93
4	2,300	0.1303	0.0091	0.070	0.197	0.0183	0.0167	33.30	13.26	45.16	20.04	-11.86
5	2,300	0.1303	0.0130	0.100	0.138	0.0550	0.0250	34.90	13.85	50.76	21.05	-15.86
6	2,300	0.1303	0.0130	0.100	0.138	0.0367	0.0167	27.80	11.70	40.20	16.10	-12.40
7	2,388	0.1255	0.0031	0.025	0.400	0.0058	0.0045	47.90	17.19	54.64	30.71	-6.74
8	2,388	0.1255	0.0031	0.025	0.632	0.0048	0.0050	55.00	17.02	53.63	37.98	1.37
9	2,388	0.1255	0.0031	0.025	0.496	0.0042	0.0045	48.10	16.68	50.65	31.42	-2.55
10	2,388	0.1255	0.0031	0.025	0.632	0.0041	0.0038	50.70	16.15	48.12	34.55	2.58
11	2,388	0.1255	0.0048	0.038	0.085	0.0058	0.0063	29.30	14.22	42.11	15.08	-12.81
12	2,388	0.1255	0.0048	0.038	0.48	0.0058	0.0063	42.20	14.22	42.51	27.98	-0.31
13	2,388	0.1255	0.0064	0.051	0.316	0.0100	0.0125	40.90	14.07	46.99	26.83	-6.09
14	2,388	0.1255	0.0064	0.051	0.316	0.0079	0.0083	34.90	13.02	38.57	21.88	-3.67
15	2,388	0.1255	0.0095	0.076	0.211	0.0183	0.0167	33.90	12.93	42.94	20.97	-9.04
16	2,388	0.1255	0.0095	0.076	0.211	0.0122	0.0125	28.30	11.15	33.91	17.15	-5.61
17	2,388	0.1255	0.0095	0.076	0.227	0.0110	0.0125	28.80	11.15	32.56	17.65	-3.76
18	2,388	0.1255	0.0127	0.101	0.158	0.0220	0.0250	29.30	11.14	39.43	18.16	-10.13
19	2,388	0.1255	0.0127	0.101	0.158	0.0157	0.0167	23.30	9.79	29.77	13.51	-6.47
20	2,388	0.1255	0.0031	0.025	0.632	0.0055	0.0056	58.20	17.66	56.82	40.54	1.38
21	2,388	0.1255	0.0031	0.025	0.632	0.0041	0.0038	50.20	16.15	48.12	34.05	2.08
22	2,388	0.1255	0.0064	0.051	0.316	0.0100	0.0125	42.30	14.06	46.99	28.24	-4.69
23	2,388	0.1255	0.0064	0.051	0.316	0.0079	0.0083	35.40	13.02	38.57	22.38	-3.17
24	2,388	0.1255	0.0095	0.076	0.211	0.0183	0.0167	34.00	12.93	42.94	21.07	-8.94
25	2,388	0.1255	0.0095	0.076	0.211	0.0122	0.0125	29.30	11.15	33.91	18.15	-4.61
26	2,388	0.1255	0.0127	0.101	0.158	0.0220	0.0250	29.00	11.14	39.43	17.86	-10.43
27	2,388	0.1255	0.0127	0.101	0.158	0.0157	0.0167	23.20	9.79	29.77	13.41	-6.57
28	8,448	0.0355	0.0032	0.089	0.496	0.0042	0.0045	37.30	16.54	33.95	20.76	3.35
29	8,448	0.0355	0.0048	0.134	0.48	0.0055	0.0063	31.00	13.89	25.52	17.11	5.48
30	8,448	0.0355	0.0032	0.089	0.400	0.0052	0.0050	36.00	17.29	37.87	18.71	-1.87
31	8,448	0.0355	0.0016	0.045	0.256	0.0020	0.0020	37.60	19.16	39.90	18.44	-2.30
32	8,448	0.0355	0.0048	0.134	0.085	0.0055	0.0063	17.70	13.91	25.12	3.79	-7.42
33	8,448	0.0355	0.0016	0.045	0.048	0.0020	0.0020	30.90	19.16	39.70	11.74	-8.80

[1]Actual measurements per Otoshi 1972 paper.

[2]Probabilistic results using equation (13).

[3]The Otoshi Model, equation (18) results, calculated using reconstructed number of holes in the perforated sheet.

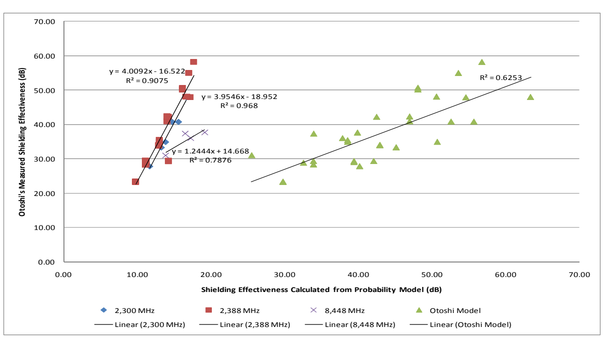

(a)

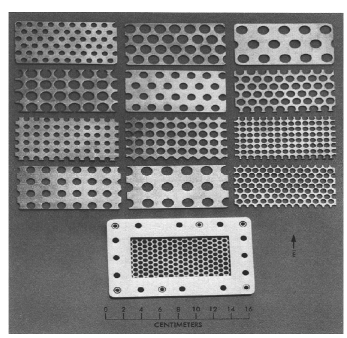

(b)

Figure 9. (a) Measured versus probabilistic shielding and (b) Otoshi's sample perforated sheets & holder (JPL, 1972).

TESTING THE CLOAKING HYPOTHESIS

Figure 10(a), uncloaked & 10(b), cloaked, show Schurig *et al.* (2006) microwave patterns. Schurig's microwave cloaking movies S3 and S4 show that cloaking is the ability *go around* objects and is the opposite of shielding. This *going around* within the cloaking material is visible in Figure 10(b). The color coding shows that the electromagnetic wave substantially travels through the cloaking material before exiting the other side. It takes a longer path and is more compressed and apparently faster than the wave structure outside the cloaking material. In Figure 10(a) by comparison, the electromagnetic wave is traveling slower than the wave outside the Cu cylinder.

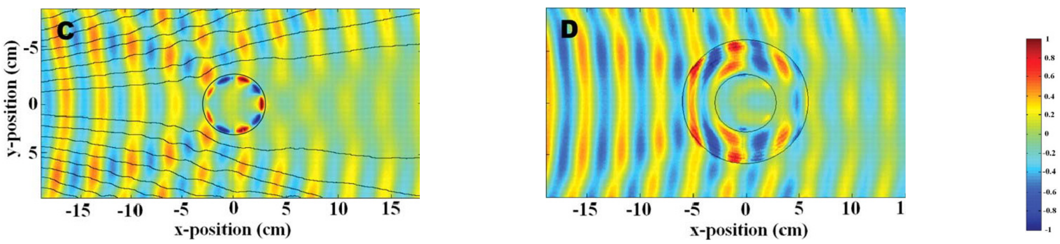

(a) **(b)**

Figure 10. (a) Cu distorts exiting wave patterns on right and (b) Cloaked Cu cylinder's minimal distortion (**Science 12/10/2006**).

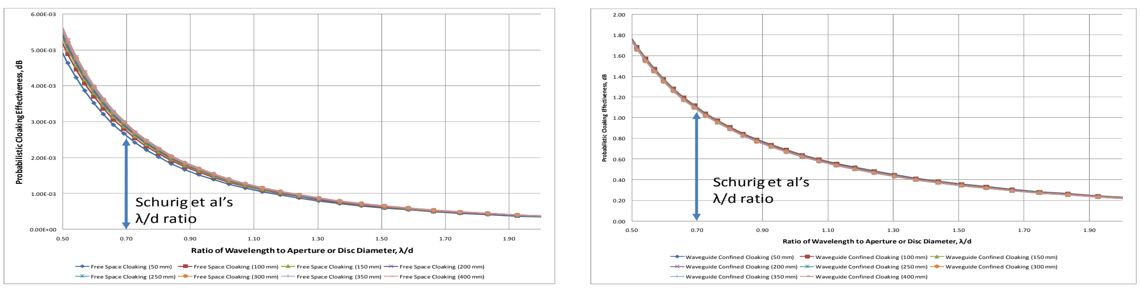

(a) **(b)**

Figure 11(a) Free space cloaking efficiency and (b) confined space cloaking efficiency.

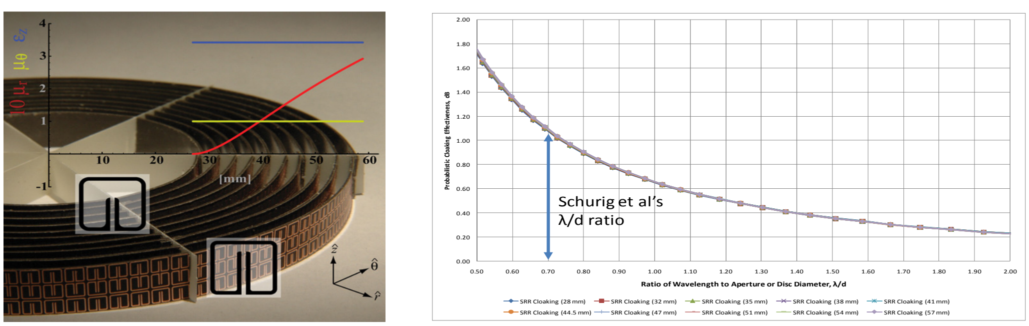

(a) **(b)**

Figure 12 (a): Schurig's SRR rings (**Science 12/10/2006**) and (b): SRR cloaking efficiency.

As a control, Figures 11(a) and (b), equation (15) was used to calculate the cloaking effectiveness CE_P for a microwave cavity that resembles Schurig's, 11mm high, 200mm wide ($R=100mm$) and 400mm long ($D_P=50mm$ to $400mm$ in increments of $50mm$), assuming a coaxial cable radius of about 2mm ($D_A\approx 2mm$), and a frequency of 8.5 GHz. These controls show that free space $CE_P\approx 5x10^{-3}dB$ when $\lambda/d\geq 0.5$. Abbe's diffraction limit which determines the smallest features one can see (Zhang *et al.*, 2008) at $\lambda/d\geq 2$ sets $CE_P\approx 3.6x10^{-4}dB$. Probabilistic Cloaking provides a different approach to the photon's resolution limit that diffraction could be a probabilistic phenomenon. However, when confined to the microwave cavity, the decibels increase dramatically to $1.1dB$ but are still low for $\lambda/d=0.7$. To estimate the effect of SRR ring square, the CE_P in a confined space was calculated for $D_A=1.5mm$ (half of the SRR ring square edge length of 3mm), for each distance from the outer ring, Figure 12(a) to each subsequent inner ring (*D_P=28, 32,… 54, 57mm*) approximating the orthogonal cross-section of 200mm to an equivalent radius, *R=100mm*, frequency of 8.5 GHz. The results, Figure 12(b), show that for *λ/d =0.7*, *CE_P* ranges between *1.09dB* and *1.12dB* or the same as the waveguide's characteristics. Schurig's experiment provides an important marker, that for *confined cloaking* to be effective *$CE_P \leq 1.1dB$*. This analysis suggests that the multi-layer SRR type material design would provide an effective microwave *shield* by causing the photon to propagate along the material rather than through it. Similar design strategies could be used for other types of radiation shielding.

INVISIBILITY MODEL

In shielding the unwanted phenomenon is the proportion of the photon probability distribution that lies within the aperture. In invisibility this is the primary phenomenon, with the intent to maximize the photon probability distribution that passes through an aperture. This is accomplished by squeezing the probability distribution. Figures 13(a) and (b) graph the results of a microwave invisibility (*D_P=0.1m, R=0.2m*, *height=11mm at 8.5 GHz*) while reducing D_A by one order of magnitude (*$D_A=1.5x10^{-1}m$, $1.5x10^{-2}m$,… and $1.5x10^{-6}m$*). The free space Invisibility Effectiveness equation (18) shows that reducing the size of D_A is a method to achieving invisibility, but invisibility is not possible *$IE_P<0$*, as there is a limit to how much D_A can be reduced. In a confined space, equation (17), *$IE_P>0$* for any λ/d<0.5. This is not a surprising result but more importantly Probabilistic Invisibility concurs with common sense observations. The graphs show that invisibility in a confined space dependent on the shape of the confinement and the results can be of mixed usefulness. This modeling suggests that invisibility cannot be achieved by 'mechanically' squeezing the photon by reducing D_A. Invisibility requires a technologically more sophisticated method derived from the understanding of how an electromagnetic field casts a shadow on the photon distribution.

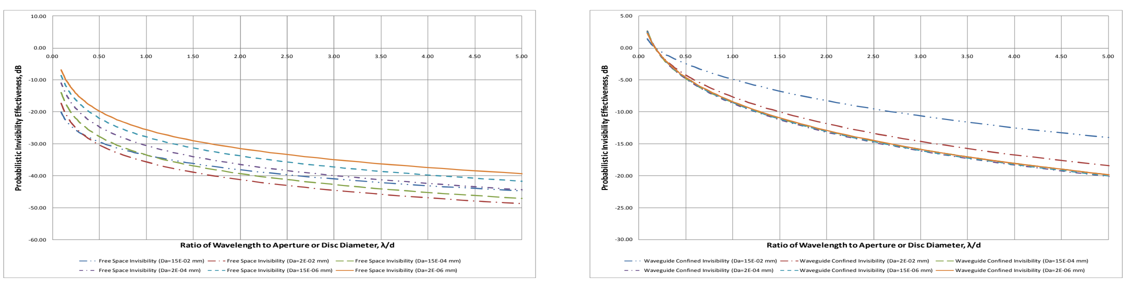

(a) **(b)**

Figure 13. (a) Free space invisibility effectiveness and (b) confined space invisibility effectiveness.

SUBWAVELENGTH CONFINEMENT

Oulton *et al.* (2008) researched THz (*λ=1,550nm*) photon propagation along a dielectric cylindrical GaAs nanowire of diameter *d* embedded in SiO_2 at a distance *h* from a metallic region using hybrid waveguide. Their experiments show that one can increase propagation distance while maintaining moderate confinement by tuning the geometric properties of the encased nanowire. To test how Probabilistic Interaction Hypothesis, equation (12) and *mΓ* distribution stands up at subwavelength confinement a numerical model was built treating the optical photon in a nanowire as equivalent to a confined radio wave photon in an antenna because the *λ/d* ratios are large in both cases. The nanowire is treated as a cylindrical electrified surface with field lines stretching out to the metal plane due to the transverse electromagnetic wave (Elmore and Heald, 1985) and therefore the electrical field strength decreases inversely with distance from the edge of the nanowire to the metal plane. The electric field E_I inside (radius r_I) and E_O (radius r_O) outside the cylindrical nanowire and the electric field energy density *η* at a distance *r* are given by equations (29), (30) and (31) respectively, for a charge per unit length *q*, with dielectric constants *ε_I=12.25*, *ε_O=2.25* and *ε_M=129* for GaAs nanowire, SiO_2 upper medium, and lower metallic plane, respectively

$$E_I = \left(q/2\pi\varepsilon_I\right) r_I \Big/ \left(d/2\right)^2 \; ; \tag{29}$$

$$E_O = \left(q/2\pi\varepsilon_O\right) \big/ r_O \; ; \tag{30}$$

$$\eta = \left(1/2\right)\left(\varepsilon E^2 A r\right) . \tag{31}$$

Schurig *et al.* (2006) experimental results, Figure 11(b), suggest energy intensification per unit volume occurs in a confined environment. As λ/d is large ($155 \leq \lambda/d \leq 775$) this intensification is not modeled as an effect of the field strength but due to the increase in the probability density function resulting from the confinement barriers. Given that the photon does not actualize at the barrier, the confined radial probability P_{cr} is scaled up so that the sum of the confined probabilities along a radius is *1* per equation (32). Therefore, the confined energy density is ηP_{cr} which takes the form of the Probabilistic Interaction Hypothesis, equation (12) with $A_i = \eta$, $f(P_i) = P_{cr}$ and $B_i = 0$

$$P_{cr} = P_r \left(\sum_{0 \leq r \leq \infty} \delta r P_r \Big/ \sum_{0 \leq r} \delta r P_r \right) = P_r \left(1 \Big/ \sum_{0 \leq r} P_r \right) \tag{32}$$

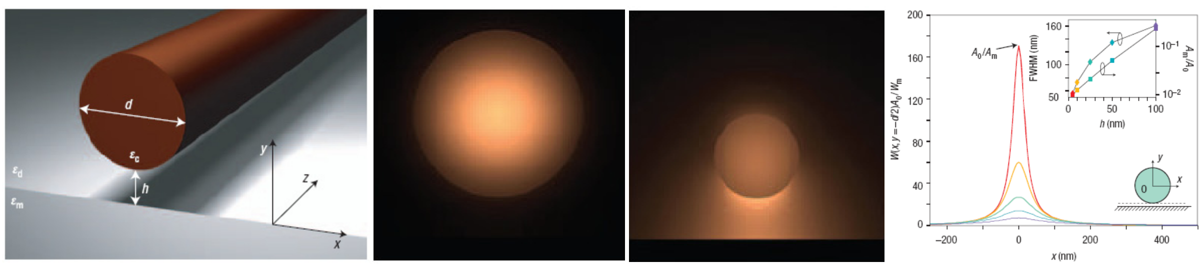

(a) **(b)** **(c)** **(d)**

Figure 14. (a): Nanowire, (b): Energy distribution at [d,h]=[400,100] nm,(c): Energy distribution at [d,h]=[200,100] nm and (d): Energy distribution parallel to metal plane. (**Nature Photonics**)

Oulton data, Figure 14, is presented as normalized intensities, thus for comparisons, distribution of electromagnetic energy in the modified Gamma hypothesis ($D_A = d/2$) is calculated as the probability P_r at a distance r from the center of the nanowire. Comparing the numerical model results with Oulton's shows that even though the probability distribution, Figure 15(a), is equivalent to the electromagnetic energy, Figure 14(b), when *d= 400nm*, the gap energy shown in Figure 14(c) is not reflected in the $m\Gamma$ distribution of Figure 15(b), when *d=200nm*. This gap energy is therefore an electromagnetic function effect overlaid over the $m\Gamma$ probabilistic effect and concurs with Oulton *et al.* (2008) that there is capacitor-like energy storage between nanowire and metal plane. Figure 15(c) (*h=200nm*) and (d) (*h=2nm*). The numerical modeling shows that the two models agree in that shapes of the distribution of energy over the SiO_2 medium are similar. Especially note that the peaking behavior of the energy distribution adjacent to the metal plane, bottom left of Figures 15(c) & (d) matches Oulton's, Figure 14(d), in that the peak is higher when *h=2nm*, and drops as *h* get larger to *200nm*. However, there is a significant difference in the models. The Oulton *et al.* model requires energy increase as internal metal nanowire radius decreases, while the probabilistic hypothesis treats this as a known electromagnetic skin effect.

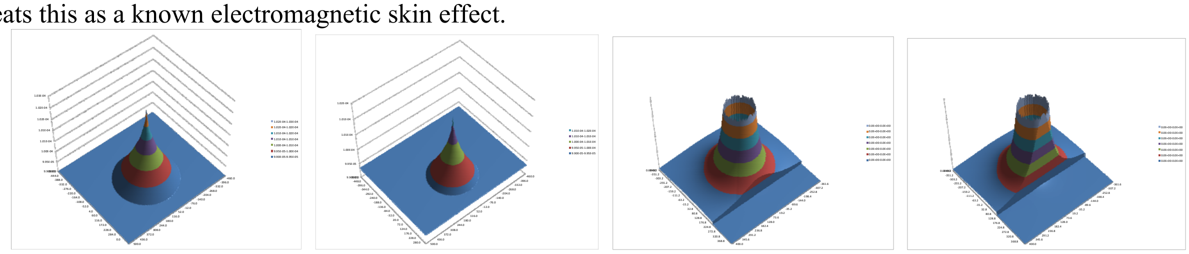

(a) **(b)** **(c)** **(d)**

Figure 15. (a) mΓ probability distribution at [d,h]= [400,100] nm, (b) mΓ probability distribution at [d,h]= [200,100] nm, (c) model linear energy distribution at [d,h] = [200,100] nm and (d) model linear energy distribution at [d,h]= [200,2] nm.

CONCLUSION

Numerical modeling based on empirical evidence was used to show that the photon's probability distribution is a modified Gamma distribution whose parameters are the orthogonal and forward distances of the space around the photon. Not only is the photon's probability distribution altered by the shapes of space around it but this paper, using available experimental data, has made the case that a photon's response to the materials around it is related to the geometric proportions as a ratio of its wavelength. The modified Gamma distribution provides an alternative explanation for optical resolution, lends itself to a unified shielding, cloaking and invisibility hypothesis, and may even replace the sum of histories method. More importantly it presents shielding, cloaking and invisibility as distinctly different interactions of the same phenomenon. The shielding and cloaking models concur with the experimental data. The invisibility model suggests the need for a better understanding of the photon. The nano wire model shows that the skin effect can be used to model sub wavelength behavior. In summary this paper has presented a substantial body of evidence to make the case that a photon's probability distribution is a modified Gamma distribution.

NOMENCLATURE

I = Intensity
I_O = Reference intensity
λ = wavelength of light photon
D_A = aperture diameter of the pinhole
D_P = distance between pinhole & screen
r = Airy pattern radius
θ = angle formed by D_P and r
u = Airy disc parameter
$m\Gamma$ = modified Gamma distribution
I_i = Probabilistic Interaction Hypothesis
A_i = accelerant or interaction factor
B_i = barrier
α = the continuous shape parameter
β = the continuous scale parameter
d = diameter of aperture or disc
$R_{1\%}$= radius of photon at 1% probability
$L_{1\%}$= length of photon at 1% probability
$P_{i,x,y,z}$ = probability of photon i at (x,y,z)
$P_{j,x,y,z}$ = probability of photon j at (x,y,z)
$P_{i,j}$ = joint probability of photon i and j
SE_P = Shielding Effectiveness
CE_P = Cloaking Effectiveness
IE_P = Invisibility Effectiveness
r = inner or smaller radius
R = outer or larger radius
$P_{\leq R}$ = probability within radius R
$P_{\leq r}$ = probability within radius r
$P_{>r}$ = probability outside radius r
a, b & c = some constants
x_i = ith distance between 0 and r
δr = increment in the radial distance
h = microwave cavity height
t = plate thickness
a & b = distances between holes
T_{dB} = Otoshi's transmission loss
SE_L = Shielding Effectiveness
E_I = electric field inside nanowire
E_O = electric field outside nanowire
η = electric field energy density
q = charge per unit length
ε_I, ε_O and ε_M = dielectric constants

REFERENCES

Aspect, A., Dalibard, J. and Roger, G., "Experimental Test of Bell's Inequalities Using Time-Varying Analyzer," *Phys. Rev. Lett.*, **49**(25), (1982), pp. 1804 – 1807.

Eisaman, M. D., Goldschmidt, E. A., Chen, J., Fan, J. and Migdall, A., "Experimental test of nonlocal realism using a fiber-based source of polarization-entangled photon pairs," *Phys. Rev. A*, **77**, (2008), p. 032339.

Elmore, W. C. and Heald, M.A., *Physics of Waves*, Dover Publications, New York, (1985), p. 241.

Howell, J. C., Bennink, R. S., Bentley, S. J. and Boyd, R. W., "Realization of the Einstein-Podolsky-Rosen Paradox Using Momentum and Position-Entangled Photons from Spontaneous Parametric Down Conversion," *Phys. Rev. Lett.,* **92**(21), (2004), pp. 210403-1-4.

Leach, J., Jack, B., Romero, J., Rirsch-Marte, M., Boyd, R. W., Jha, A. K., Barnett, S. M., Franke-Arnold, S., and Padgett, M. J., "Violation of a Bell inequality in two-dimensional orbital angular momentum stat-spaces," *Optics Express*, **17**(10), (2009).

Otoshi, T. Y., "A study of microwave transmission through perforated flat plates," JPL Technical Report, 32-1526, Vol. II, (1972).

Schurig, D., Mock, J. J., Justice, B. J., Cummer, S. A., Pendry, J. B., Starr, A. F., Smith, D. R., "Metamaterial Electromagnetic Cloak at Microwave Frequencies," *Science*, **314**(5801), (2006), pp. 977 – 980.

Schurig, D., Mock, J. J., Justice, B. J., Cummer, S. A., Pendry, J. B., Starr, A. F. and Smith, D. R., "Metamaterial Electromagnetic Cloak at Microwave Frequencies," *Science*, 10 December, (2006).

Solomon, B. T., "An Approach to Gravity Modification as a Propulsion Technology, in the *Space, Propulsion & Energy Sciences International Forum (SPESIF-2009)*, edited by G. A. Robertson, AIP conference proceedings **1103**, Melville, NY, (2009).

Tittel, W., Brendel, J., Gisin, B., Herzog, T., Zbinden, H., and Gisin, N., "Experimental demonstration of quantum-correlations over more than 10 kilometers," *Phys. Rev. A*, **57**, (1998), p. 3229.

Yao, E., Franke-Arnold, S., Courtial, J. and Padgett, M. J., "Observation od quantum entanglement using spatial light modulators," *Optics Express*, **14**(26), (2006).

Yarnall, T., Abouraddy, A. F., Saleh, B. E. A. and Teich, M. C., "Experimental Violation of Bell's Inequality in Spatial-Parity Space," *Phys Rev. Lett*., **99**, (2007), p. 170408.

Zhang, X. and Liu, Z., "Superlenses to overcome the diffraction limit," Nature Materials, **7**, (2008), p. 435.

Oulton, R.F., Sorger, V.J., Genov, D.A., Pile, D.F.P. and Zhang, X., “A hybrid plasmonic waveguide for subwavelength confinement and long-range propogation,” Nature Photonics, **2**, August 2008